Modification of microneedles using inkjet printing

R D Boehm,[1] P R Miller,[1] S L Hayes,[1] N A Monteiro-Riviere,[1,2] and R J Narayan[1,a]

[1]*Joint Department of Biomedical Engineering, University of North Carolina and North Carolina State University, Raleigh, NC 27695-7115, USA*

[2]*Center for Chemical Toxicology Research and Pharmacokinetics, Department of Clinical Sciences, North Carolina State University, Raleigh, NC 27695, USA*

(Received 15 April 2011; accepted 28 May 2011; published online 10 June 2011)

In this study, biodegradable acid anhydride copolymer microneedles containing quantum dots were fabricated by means of visible light dynamic mask micro-stereolithography-micromolding and inkjet printing. Nanoindentation was performed to obtain the hardness and the Young's modulus of the biodegradable acid anhydride copolymer. Imaging of quantum dots within porcine skin was accomplished by means of multiphoton microscopy. Our results suggest that the combination of visible light dynamic mask micro-stereolithography-micromolding and inkjet printing enables fabrication of solid biodegradable microneedles with a wide range of geometries as well as a wide range of pharmacologic agent compositions. *Copyright 2011 Author(s). This article is distributed under a Creative Commons Attribution 3.0 Unported License*. [doi:10.1063/1.3602461]

I. INTRODUCTION

Microneedles are small-scale needle-shaped devices in which one dimension of the device is less than 500 μm in length. These devices are used to produce pores in the 15 μm-thick stratum corneum. This superficial layer of skin contains nonviable keratinized cells bathed in lipids; it functions as a primary barrier to transport of pharmacologic agents.[1–3] Microneedles are commonly used to deliver charged, polar, or large pharmacologic agents (e.g., nucleic acid-containing agents) since these agents cannot be delivered in enteral form due to first-pass metabolism and/or pH-driven degradation.[4–6] Gill *et al.* showed that microneedles are associated with less pain than 26-gauge hypodermic needles; this result is attributed to the fact that microneedles have fewer interactions with Pacinian corpuscles, Meissner's corpuscles, and nerve endings in the dermis than conventional hypodermic needles.[7] Due to the small dimensions of microneedle devices, tissue damage at the injection site is also minimized; this feature is useful for treatment of diabetes and other chronic medical conditions that necessitate frequent injections.[8] Furthermore, no specialized medical training is necessary for microneedle use. Common drug delivery mechanisms involving microneedle devices include: (a) coating solid microneedles with one or more pharmacologic agents and inserting the coated microneedles into the skin; (b) flowing a liquid that contains one or more pharmacologic agents through the bores of hollow microneedles; and (c) puncturing the skin with microneedles and subsequently delivering one or more pharmacologic agents at the microneedle site by means of a patch.[9] Dip coating is commonly used to prepare coatings on microneedles and other structures with complex geometries.[10] In dip coating, microneedles are dipped and withdrawn from a solution that contains the coating material; upon drying, a coating is obtained on the microneedle surface.

Use of coated solid microneedles has been investigated by several researchers. For example, Cormier *et al.* demonstrated delivery of desmopressin to a hairless guinea pig model by mean

[a]Email address: roger_narayan@unc.edu; Telephone: 919 696 8488; FAX: 919 513 3814

of a titanium microneedle array; in this study, the microneedles were coated with 24 or 40 wt.% desmopressin and 0.2 wt.% polysorbate using a partial immersion process.[11] They noted that the partial immersion process resulted in creation of some contaminated microneedle arrays, in which the coating extended to the microneedle base. Although good microneedle-to-microneedle coating uniformity was noted, the distribution of the coating was not uniform throughout the microneedle structure. Matriano *et al.* coated ovalbumin solution onto titanium microneedle arrays. Ovalbumin in the coating interacts with immune cells within the skin; high antibody titers were obtained in a hairless guinea pig model using these devices.[12] Subsequent work showed that coating only the topmost 100 μm of the microneedle tips within a microneedle array instead of the entire microneedle array increased the delivery efficiency from 4-14% to 48%-58%.[13]

It should be noted that several limitations are associated with conventional solid microneedle coating mechanisms. For example, the total amount of pharmacologic agent loaded on the microneedle is constrained by the microneedle surface area.[9] Gill *et al.* described a dip-coating process involving dipping, withdrawal, and drying stages.[14] Gill *et al.* used non-aqueous solvents and surfactants in order to reduce surface tension, improve wetting, and increase coating uniformity. They also indicated that viscosity enhancers, including acacia, sodium alginate, carboxymethylcellulose, hyaluronic acid, polyvinylpyrollidone, sucrose, and xanthan gum, may be used to increase the coating thickness. In another study, Gill *et al.* increased coating thickness and uniformity by including the surfactant Lutrol F-68 NF and the viscosity enhancer carboxymethylcellulose in the coating solution; they successfully coated macromolecules, small molecules, and microparticles on microneedle surfaces using this approach.[10] In addition, they created a specialized procedure, which involved masking and micropositioning, for eliminating interactions between the microneedle substrate and the coating solution. More recently, Chen *et al.* increased coating solution viscosity with sodium alginate; they demonstrated nanopatch-based delivery of ovalbumin protein and DNA using this approach. It should be noted that surface tension-related processes may serve to spread the microneedle coating to portions of the microneedle device (e.g., the microneedle substrate) where it is not needed[15]

Gill *et al.* noted that increasing microneedle-to-microneedle dosage uniformity and minimizing waste of expensive pharmacologic agents are important considerations in the development of a microneedle coating process.[10] Chen *et al.* and Gill *et al.* described several attributes of an ideal microneedle coating process; these include: (a) minimizing deposition of the coating material on the microneedle substrate, (b) minimizing heating or pH changes for the coating material, and (c) maximizing adhesion between the coating material and the microneedle material.[10,15] Chen *et al.* also noted that an ideal microneedle coating approach should be suitable for scalable, industrial-scale processing.[15]

Inkjet printing may serve as an alternative approach for modifying the surfaces of microneedles. Inkjet printing is a non-contact process that has been used for dispensing picoliter volumes of biologically-relevant materials, including proteins and nucleic acids, in a drop-on-demand manner.[16–18] Kim *et al.* described inkjet printing as a "dosing robot" that generates microscale patterns with arbitrary geometries.[19] Furthermore, coatings can be deposited at room temperature on a wide variety of materials, including temperature-sensitive polymers and fabrics.[20] Abe *et al.* and Allain *et al.* noted that piezoelectric inkjet printing is associated with low contamination rates and high reproducibility rates, respectively.[21,22] In addition, Dzik *et al.* noted that inkjet printing is associated with low cost and low rates of material waste.[23] They also showed that materials can successfully be patterned without use of a wetting agent. High inkjet printing rates have been demonstrated; for example, Lin *et al.* described inkjet processing rates as high as 10^{-2} m/s.[24] Cerna *et al.* noted that inkjet printing is more efficient process for creating coatings than dip coating.[16] Mosiadz *et al.* noted that dip coating suffers from coating-to-coating nonuniformity; inkjet printing provides greater control over coating amount.[25] In piezoelectric inkjet printing, a container containing a dispersion or solution is surrounded by a piezoelectric actuator.[26] In this study, the container includes a silicon diaphragm, which is attached to patterned lead zirconate titanate transducer. Voltage pulses lead to sub-micrometer scale contraction and expansion of the transducer; the pressure wave associated with this motion leads to droplet release from a nozzle. The droplet size is related to the nozzle dimensions. Deformation of the piezoelectric actuator is associated with bend, push, squeeze, or

shear motions.[27] The cartridge used in this study contains a bender mode printer head; transducer actuation takes place in the wafer plane. Increases in the applied voltage are associated with increases in droplet impact force, velocity, and mass. Unlike thermal inkjet printing, piezoelectric inkjet printing does not involve heating of the dispersion or solution. Piezoelectric inkjet printing also provides greater control over generation of the pressure pulse and ejection of the droplet than thermal inkjet printing.

A variety of materials, including glass, silicon, metals (e.g., nickel), metal alloys (e.g., stainless steel), non-biodegradable polymers (e.g., acrylate-based polymers) and biodegradable polymers (e.g., polylactic acid), have been used in microneedle fabrication.[28–31] Using microneedles that are fabricated out of non-biodegradable materials is problematic because broken microneedles may be retained within the skin. In this study, microneedles were fabricated out of a biodegradable acid anhydride copolymer (CAS 9011-16-9) containing alternating maleic anhydride and methyl vinyl ether groups, which is sold under the tradename Gantrez® AN-139.[32] Gantrez materials are soluble in organic solvents (e.g., aliphatic esters, alcohol, and phenols) as well as water. It should also be noted that Gantrez AN materials exhibit solubility as well as stability in water over the complete pH range; the solubility of Gantrez AN materials in water is constrained by the viscosity of the solution. Gantrez® AN-139 was first commercially distributed by General Aniline and Film Corporation in 1961; it is currently distributed by International Specialty Products, Incorporated.[33] Lappas and McKeehan described the use of poly(methylvinyl ether-co-maleic anhydride) as a coating for enteric and sustained-release applications.[32] Infrared spectroscopy, turbidity point, and electrometric titration studies indicated no thermal instability in materials that were aged at 50° C. Chronic and acute toxicology studies indicated that the material is nontoxic. Irache *et al.* noted that the oral toxicity of Gantrez® AN polymers is quite low; in the guinea pig, the LD_{50} was noted to be 8-9 g/kg per os.[34]

Glicksman described use of this material in a variety of pharmaceutical and cosmetic products, including ointment thickening agents, denture stabilizers/fixatives, detergents, hair sprays, lotions, and shampoos.[33] Corzani described use of Gantrez® AN-139 for reducing odor in hygienic articles; he noted that Gantrez® AN-139 exhibits anti-bacterial properties comparable to those of antibiotics, including norfloxacin, netilmicin, ceftriaxone, ceftazidime, and amoxicillin/clavulanic acid.[35] Using in vitro studies, Gantrez® AN-139 was shown to prevent growth of *Escherichia coli*, *Staphylococcus aureus*, *Streptococcus* spp., *Pseudomonas aeruginosa*, *Proterus vulgaris*, and *Aspergillus niger*. The antimicrobial properties of Gantrez® AN-139 may be useful for minimizing movement of microorganisms through microneedle-fabricated pores.[1,36,37] Date *et al.* prepared nanoparticles containing the anti-tuberculosis agent rifmapicin, the complexing agent dioctyl sodium sulfosuccinate, and the polymer Gantrez® AN-119 by means of an emulsion-solvent diffusion protocol.[38] Fructose and trehalose were shown to function as cytoprotectants; the cytoprotection functionality was proportional to the cytoprotectant concentration. These nanoparticles demonstrated rifampicin release rates that corresponded with diffusion kinetics. Poly (methyl vinyl ether-co-maleic anhydride) materials are commonly used for oral drug delivery due to the fact that these materials facilitate gut mucosa interactions and increase the bioavailability of pharmacologic agents. Elizondo *et al.* noted that use of polyanyhdride nanoparticles for oral drug delivery has been approved in the United Kingdom.[39] They utilized a compressed antisolvent protocol for creating gentamicin-loaded Gantrez® AN-119 nanoparticles; the efficacy of the composite nanoparticles against a facultative intracellular organism, *Brucella melitensis*, was demonstrated. Nabi *et al.* described preparation of a detrifice containing Gantrez® and triclosan; the Gantrez®-triclosan dentrifice was associated with higher rates of triclosan uptake to enamel and buccal epithelial cells than the triclosan dentrifice.[40] A dentrifice containing 2.0% PVM/MA copolymer, 0.3% triclosan, and fluoride (Colgate® Total®Toothpaste) was subsequently developed to provide protection against caries, malodor, plaque, and periodontal disease progression.[41] More recently, Donnelly *et al.* created microneedles with heights of 600 μm and 900 μm out of Gantrez® AN-139 using a laser-based micromoulding method; solid microneedles containing 1% (w/w) theophylline were noted to be not flexible.[42] Penetration of porcine skin was demonstrated; delivery of theophylline was observed using high performance liquid chromatography. In contrast, they noted that Gantrez® AN-139-theophylline mixtures containing above 1% (w/w) theophylline were flexible and unsuitable for microneedle fabrication. In another study,

Donnelly *et al.* delivered a model drug, Nile red, using Gantrez® AN-139 microneedles.[43] The hydrophobic model drug was encapsulated within 150 nm diameter poly(lactic-co-glycolic acid) nanoparticles. Nile red was observed in low levels within excised porcine skin sections that were obtained from unpunctured skin. On the other hand, high concentrations of Nile red were noted in microneedle-treated skin.

A quantum dot solution was selected as a model drug due to its unique potential as a fluorophore and as a drug delivery vehicle. Quantum dots are fluorescent semiconductor nanocrystals with diameters between 2 nm and 10 nm.[44–48] These nanoparticles exhibit quantum confinement due to the fact that the nanoparticle radius is smaller than the exciton Bohr radius (average electron-hole distance); due to quantum confinement, quantum dots exhibit larger bandgap values than bulk material as well as characteristic excitation states. Quantum dots exhibit unusual photoluminescence properties, including higher resistance to photobleaching (light-dependent oxidation). In addition, quantum dots exhibit high brightness values, which are associated with large molar extinction coefficient values and high quantum yield values. Quantum dots may be utilized in tumor treatment; passive quantum dot-tumor cell interactions (e.g., preferential retention of quantum dots within tumor cells) and active quantum dot-tumor cell interactions (e.g., conjugation of quantum dots with antibodies, aptamers, peptides, and/or pharmacologic agents) have been described in the literature.[49–54]

In this study, solid biodegradable acid anhydride copolymer microneedle devices containing quantum dots were fabricated by means of visible light dynamic mask micro-stereolithography-micromolding and inkjet printing. Nanoindentation was performed to obtain the hardness value and the Young's modulus value of the biodegradable acid anhydride copolymer. Imaging of quantum dot delivery within porcine skin was accomplished by means of multiphoton microscopy. This study suggests that the combination of visible light dynamic mask micro-stereolithography-micromolding and inkjet printing may provide a unique approach for fabricating polymeric microneedle arrays, which may be used for transdermal delivery of a wide variety of pharmacologic agents.

II. EXPERIMENTAL PROCEDURE

The master structures of the microneedle arrays were fabricated in a layer-by- layer manner using a Perfactory III SXGA+ visible light dynamic mask micro-stereolithography system (EnvisionTEC GmbH, Gladbeck, Germany). This commercial rapid prototyping system utilizes a Digital Micromirror Device (DMD™) to achieve selective polymerization of a photosensitive material. The part fabrication time for visible light dynamic mask micro-stereolithography is minimized since an entire layer of material is polymerized at once. The system contains a large build envelope, which may allow multiple structures to be fabricated in a parallel manner. Several investigators have described the use of visible light dynamic mask micro-stereolithography for processing of microneedle structures. For example, Park *et al.* prepared 3×3 arrays of microcone cylinders by means of micro-stereolithography; 5 μm wide tips were demonstrated in these structures.[55] Miller *et al.* recently fabricated a hollow microneedle array out of an acrylate-based polymer; they subsequently incorporated carbon fiber electrodes within the bores of the hollow microneedles. Monitoring of ascorbic acid and hydrogen peroxide by the carbon fibers was shown.[56]

The Perfactory III SXGA+ visible light dynamic mask micro-stereolithography system is equipped with a 1280 x 1024-pixel resolution SXGA+ guidance chip (Texas Instruments, Dallas, TX) and a halogen bulb. The system was operated using a lamp power of 550 mW and a z-direction step size of 50 μm. The microneedle array master structures were fabricated within a 96.54 mm x 72.41 mm build envelope according to a layout that had been specified using Perfactory® RP software (Envisiontec GmbH, Ferndale, MI). The master structure, a 1 x 5 microneedle array on a rectangular substrate, was designed using SolidWorks Education Edition 2009-2010 (Dassault Systèmes SolidWorks Corporation, Concord, MA). The microneedle center-to-microneedle center distance was 2 mm; the dimensions of the rectangular substrate were 10 mm x 2.5 mm. Each microneedle consisted of a tip with a modified conical shape, which was located directly above a base with a modified cylindrical shape. The base exhibited a modified cylindrical shape, including a diameter of 500 μm and a height of 500 μm. This cylinder was modified by extrude-cutting a surface with a 63.4° slope through half of the cylinder width. The tip exhibited a modified

conical shape, including a base diameter of 500 μm and a height of 1000 μm. The tip exhibited a longitudinally-sliced cone shape; in this structure, the flat vertical face was aligned with the slanted face of the base. This flat vertical face facilitated deposition of quantum dot solution by means of piezoelectric inkjet printing. The microneedle array master structures were prepared using a Class-IIa biocompatible acrylate-based polymer.[57] The polymer, which is distributed under the tradename eShell 200 (Envisiontec GmbH, Ferndale, MI), is used to create water-resistant medical devices such as thin-walled hearing aid shells. Per manufacturer data, eShell 200 contains 0.5–1.5% wt phenylbis(2,4,6 trimethylbenzoyl)-phosphine oxide photoinitiator, 15–30% wt propylated (2) neopentyl glycoldiacrylate, and 60–80% wt urethane dimethacrylate. The acrylated-based polymer exhibits a water absorption value of 0.12% (D570-98 test method), a flexural strength of 103 MPa (D790M test method), a tensile strength of 57.8 MPa (D638M test method), a glass transition temperature of 109 °C (E1545-00 test method), and an elongation at yield of 3.2% (D638M test method).

The master structures were used to create molds out of Silgard® 184 polydimethylsiloxane (PDMS) (Dow Corning, Midland, MI). Each master structure was sputter-coated for three minutes with a layer of 60% gold-40% palladium using a Technics Hummer II instrument (Anatech, Battle Creek, MI). The base was adhered to a small strip of aluminum using Loctite® 404™, a cyanoacrylate adhesive (Henkel, Rocky Hill, CT). A 20 mm diameter aluminum crimp top seal washer was wrapped in aluminum foil and filled with 5 mL of PDMS; a 1:10 curing agent: elastomer ratio was used in this study. The master structure was subsequently suspended upside down on the aluminum ring while being dipped into the PDMS resin. This construct was placed on a 125°C hotplate for ten minutes to facilitate polymerization of PDMS. The master structures were subsequently removed from the molds using forceps.

Gantrez® AN-139 was obtained from a commercial source (International Specialty Products, Wayne, NJ).[58] Per the manufacturer, the as-prepared material is a water-insoluble white powder that is readily dispersed in water; hydrolysis of the anhydride results in formation of a transparent solution, which contains the soluble free acid. Gantrez® AN-139 exhibits a nominal molecular weight of 1.0 x 10^6 and a T_g of 151° C. Rowe *et al.* noted that Gantrez® AN-139 exhibits a bulk density of 0.33 g/cm^3 and a polydispersity of 3.47 (Mn/Mw).[59] A 20% w/w aqueous gel material was created using the as-received powder and deionized water by means of heating and sonication. To create microneedle arrays out of Gantrez® AN-139, the PDMS molds were filled with the aqueous gel material. The molds were subsequently centrifuged at 3500 rpm for fifteen minutes. The molds were then allowed to dry overnight at room temperature. Following drying, the molds were filled with additional material. The molds were subsequently centrifuged at 3500 rpm for fifteen minutes. The molds were then allowed to dry overnight at room temperature. The Gantrez® AN-139 microneedle arrays were subsequently removed from the PDMS molds using forceps.

A Qtracker® 705 non-targeted quantum dot solution (Invitrogen, Carlsbad, CA) was patterned on the longitudinally cut surfaces of the microneedles using a Dimatix Materials Printer DMP-2831 piezoelectric inkjet printer (Fujifilm Dimatix Incorporated, Santa Clara, CA). Qtracker® non-targeted quantum dots were developed for imaging of small animal tissues; increased tissue penetration is facilitated by red-shifted emission. These heterogeneous nanoparticles consist of cadmium/selenium/tellurium cores, which are enveloped by zinc sulfide shells.[60] In addition, the nanoparticles are modified with polyethylene glycol-5000 coatings, which serve to minimize tissue immune response and nonspecific tissue interaction.[61–64] The polyethylene glycol-5000 coating may also serve to increase solubility in biologically-relevant media. The as-received material contains 2 μM quantum dots in 50 mM borate buffer and exhibits a pH of 8.3; 2 μM of the as-received quantum dot solution was diluted at a 1:10 volume ratio in 1x phosphate buffered saline. The recommended diluents for Qtracker® 705 solution are phosphate buffered saline and 0.14 M saline.[61] 1 mL of this diluted solution was transferred into a DMC-11610 printing cartridge (Fujifilm Dimatix Incorporated, Santa Clara, CA) using a syringe. The disposable cartridge used in this study exhibits a fluid capacity of 1.5 ml and contains a linear array of sixteen nozzles; the nozzle diameter is 21.5 μm and the drop volume is 10 pL. The software and the XY positioning system were used to deposit a triangle-shaped lattice of droplets containing quantum dot solution on the longitudinally cut surface of the microneedles; droplet formation, ejection, and trajectory were monitored using a

charge-coupled device camera and a stroboscopic light emitting diode array. Droplets of quantum dot solution were deposited at 28°C using a single cartridge nozzle. A drive voltage of 31.0 V was used in this study. Ten layers of quantum dot solution were deposited onto the longitudinally cut surface of each microneedle. During the inkjet printing process, the microneedle arrays were secured to a microscope slide with polymer clay; this procedure enabled the printing region of the microneedles and the droplet trajectory to be aligned.

Dried chips of material acquired from the centrifugation process were prepared for examination with Fourier transform infrared spectroscopy. Fourier transform infrared (FTIR) spectroscopy was performed on Gantrez® AN-139 material using a Nexus 470 system; this system contains a continuum scope and an OMNI sampler (Thermo Fisher, Waltham, MA). Spectrum analysis was accomplished using OMNIC™ software (Thermo Fisher, Waltham, MA). Visualization of the microneedle arrays was performed using a S-3200 variable pressure scanning electron microscope (Hitachi, Tokyo, Japan). Prior to imaging, the microneedle arrays were coated using a Technics Hummer II instrument (Anatech, Battle Creek, MI) with 60% gold-40% palladium. The height, width, and surface features of the quantum dot-coated and unmodified visible light dynamic mask microstereolithography-micromolding fabricated microneedles were determined from the digital SEM images using Photoshop® CS3 Extended software (Adobe Systems, San Jose, CA). Microneedles used for transdermal drug delivery must exhibit appropriate mechanical properties for skin insertion as well as handling by patients and health care providers. Nanoindentation was performed on dried chips of material acquired from the centrifugation process. Hardness (resistance of a material to penetration and/or plastic deformation) and Young's modulus (relative stiffness of a material against elastic deformation) values were obtained using an Ultra Nanoindentation Tester (CSM Instruments, Needham, MA). A force was applied normal to the sample surface using an B-J45 indenter with Berkovich geometry; a contact load of 20 μN, a maximum load of 2 mN, a loading rate of 4 mN min^{-1}, and an unloading rate of 4 mN min^{-1} were used in this study. Five indents were performed; after the maximum load was achieved, the normal load was reduced to facilitate partial or complete material relaxation. Load and penetration depth data were recorded during loading and unloading cycles of the test. Indentation hardness and Young's modulus of the material were obtained from the tangential slope of the curve and the indenter tip by means of the Oliver and Pharr method.[65]

Porcine skin and human skin exhibit similar morphology and thickness; due to these similarities, porcine skin is an acceptable model for human skin.[66–69] Dermatomed porcine skin of 400-500 μm was retrieved from the back of a euthanized female weanling Yorkshire pig; the skin was refrigerated at 3° C for one day between retrieval and use. To examine microneedle delivery of quantum dots into porcine skin, multiphoton laser scanning confocal microscopy was performed using a LSM-710 microscope (Carl Zeiss AG, Oberkochen, Germany). Multiphoton fluorescence microscopy is a useful technique for in situ imaging of quantum dots and other fluorophores; Larson *et al.* noted that quantum dots provide up to 47,000 Goeppert-Mayer unit multi-photon excitation cross-sections.[70,71] In multiphoton fluorescence microscopy, a fluorophore absorbs two long-wavelength photons from a femtosecond laser in a nearly simultaneous manner. In this technique, the emission wavelength is shorter than the excitation wavelength. This technique enables three-dimensional imaging of fluorophores within tissues for extended periods of time at high spatial resolutions. Kim *et al.* evaluated penetration of the stratum corneum layer by a combination of magainin and N-lauroyl sarcosine. Magainin/N-lauroyl sarcosine-mediated enhancement of fluorescein penetration into human cadaver skin was demonstrated using multiphoton microscopy.[72] More recently, Gittard *et al.* created hollow microneedle arrays out of an acrylate-based polymer using two photon polymerization.[31] They used a hollow microneedle to inject quantum dots into porcine skin; imaging of the quantum dots within porcine skin over fifteen minutes was obtained using multiphoton microscopy.

An array of quantum dot-coated Gantrez® AN-139 microneedles was applied to the dermatomed porcine skin surface. The array was held in place on the skin surface with removable adhesive putty (3M, St. Paul, MN). The skin was subsequently inverted and placed in a Petri dish; images were obtained through the backside of the dermatomed porcine skin. For comparison purposes, multiphoton laser scanning confocal microscopy was also used to examine topical application of quantum dot solution to the porcine skin surface. The quantum dots were imaged using a LSM-710 multiphoton microscope, which included a Chameleon femtosecond laser ($\lambda = 850$ nm) (Coherent,

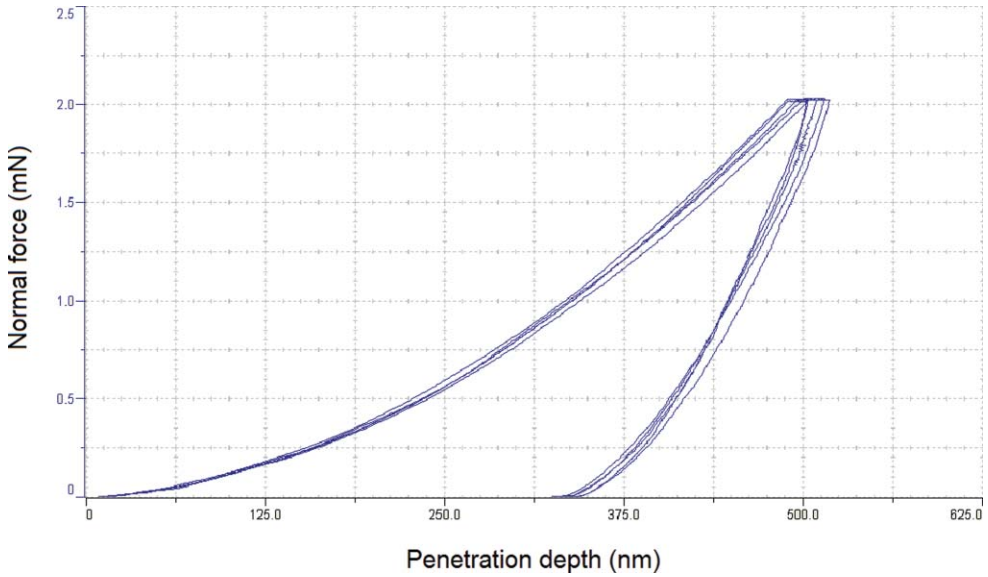

FIG. 1. Force-displacement data from nanoindentation of Gantrez® AN-139 material.

Santa Clara, CA). A 10x/0.3 EC Plan-Neofluar objective, 3.15 μs pixel dwell, and 591-728 nm filtering were used in this study. Z-stack images were created from the multiphoton laser scanning confocal microscopy data; maximum projections from the Z-stacks of quantum dot fluorescence were created using Zen 2009 Light Edition software (Carl Zeiss MicroImaging GmbH, Germany).

III. RESULTS AND DISCUSSION

Nanoindentation of the Gantrez® AN-139 material provided hardness and Young's modulus values of 385.6 +/- 12.00 MPa and 6.56 +/-0.56 GPa (data is shown as mean ± standard deviation for n=5), respectively. Figure 1 contains force-displacement data from nanoindentation of Gantrez® AN-139 material; a relatively good degree of repeatability among the indents was observed. Park *et al.* indicated that a microneedle created with a material with a Young's modulus value greater than ~1 GPa exhibits a fracture force that exceeds skin insertion forces.[73] Park *et al.* prepared microneedles out of poly-lactic-co-glycolic acid, which exhibits a Young's modulus of 3 GPa; they discussed interactions among aspect ratio, failure force, and Young's modulus.[74] The Fourier transform infrared spectrum for Gantrez® AN-139 is shown in Figure 2. The spectrum shows peaks at 2945.2 cm^{-1}, 1709.7 cm^{-1}, 1648.9 cm^{-1}, 1186.4 cm^{-1}, and 1094.2 cm^{-1}. Stretching bands associated with the anhydride group are observed at 1648.9 cm^{-1} and 1709.7 cm^{-1}; in addition, stretching bands associated with the methyl ether group are observed at 1186.4 cm^{-1} and 1094.2 cm^{-1}.[39] The broad peak at 2945.2 cm^{-1} is attributed to carbon-hydrogen stretching. The features in this spectrum closely match those of Gantrez® AN-119 methyl vinyl ether-maleic anhydride copolymer cast on calcium iodide.[75]

Figure 3 contains scanning electron micrographs of unmodified and quantum dot-coated Gantrez® AN-139 microneedles. Figure 3(a) shows a scanning electron micrograph of three unmodified Gantrez® AN-139 polymer microneedles in a five microneedle array; these microneedles were produced using visible light dynamic mask micro-stereolithography-micromolding. Figure 3(b) shows a scanning electron micrograph of three quantum dot-coated Gantrez® AN-139 polymer microneedles in a five microneedle array; these microneedles were produced using visible light dynamic mask micro-stereolithography-micromolding and piezoelectric inkjet printing. Figure 4 contains scanning electron micrographs of an unmodified Gantrez® AN-139 microneedle and a quantum dot-coated Gantrez® AN-139 microneedle. Figure 4(a) shows a scanning electron micrograph of an individual unmodified Gantrez® AN-139 polymer microneedle and Figure 4(b)

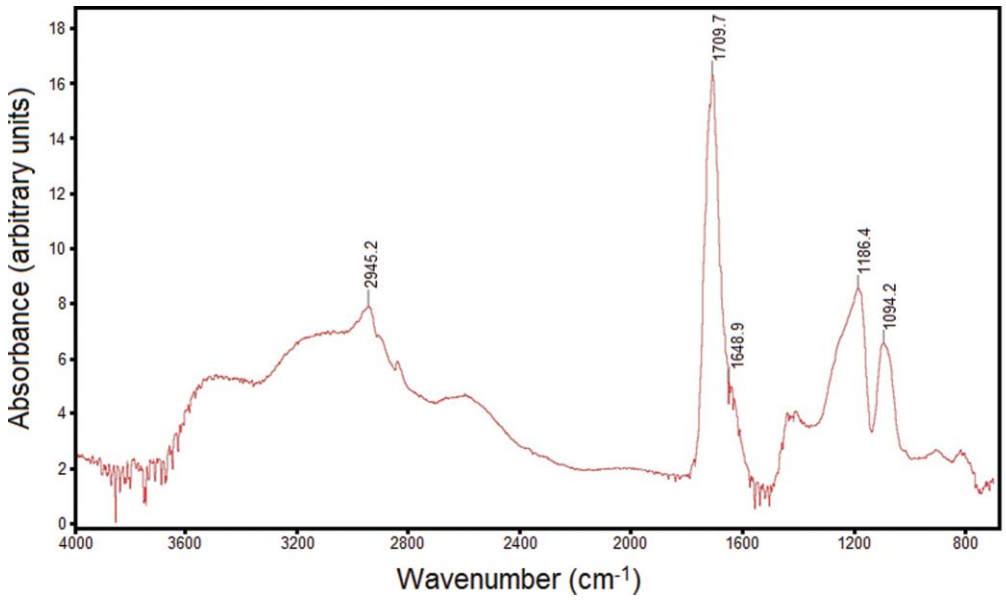

FIG. 2. Fourier transform infrared spectrum for Gantrez® AN-139 material.

shows scanning electron micrograph of an individual quantum dot-coated Gantrez® AN-139 polymer microneedle. Scanning electron microscopy data indicated that the microneedles exhibited heights of 926 ± 76 μm and base widths of 465 ± 22 μm (data is shown as mean ± standard deviation for n = 6). ~38 μm tall features were observed on the surfaces of the microneedles; these features were attributed to the spacing between the build layers in the master structure. The measurements of the microneedles are slightly smaller than the corresponding input stereolithography files. Excellent device-to-device uniformity was noted among the microneedles in the microneedle array. Microneedle arrays with greater device-to-device uniformity may be obtained by iteration of molding materials, mold fabrication parameters, and other processing parameters. The minor differences between the input dimensions and the measured dimensions were attributed to shrinkage of the Gantrez® AN-139 material within the molds as well as translation of the computer-aided design drawing by the Perfactory® RP software. Triangle-shaped regions, which contain material that was modified by the quantum dot solution, were observed on the tips of the coated microneedles. The coated microneedle exhibits crater-like features; these features were attributed to local hydrolysis of the Gantrez® AN-139 microneedle by the phosphate buffered saline solution. Sodium chloride crystal precipitation from phosphate buffered saline solution was noted on the coated microneedle surface using energy-dispersive X-ray spectroscopy. In addition, a significant difference in the cadmium concentration between quantum coated-coated region (0.58 weight percent) and the uncoated region (0.01 weight percent) was observed using energy-dispersive X-ray spectroscopy.

Figure 5 contains maximum projections rendered from acquired Z-stack multiphoton images that show (i) topical administration of quantum dots as well as (ii) Gantrez® AN-139 microneedle-based delivery of quantum dots. Figure 5(a) shows topically applied quantum dots one hour after application; in this figure, the skin was oriented with the stratum corneum at the top of the imaging window. This figure indicates that the quantum dots remained near the skin surface one hour after topical administration. Figure 5(b) shows a single quantum dot-coated microneedle one hour after application; in this figure, the image was oriented with the microneedle and the stratum corneum at the bottom of the imaging window. In Figure 5(b), the skin is positioned above the microneedle array to enable imaging; in this figure, the quantum dot signal was noted to extend >200 μm within the skin. Several investigators have examined the permeability of skin to heterogenous quantum dots. Ryman-Rasmussen *et al.* examined topical application of polyethylene glycol-amine-coated and polyethylene glycol-coated quantum dots on porcine skin; they showed that quantum dots with ellipsoid shapes and spherical shapes became localized within the epidermis layers by eight hours.[64]

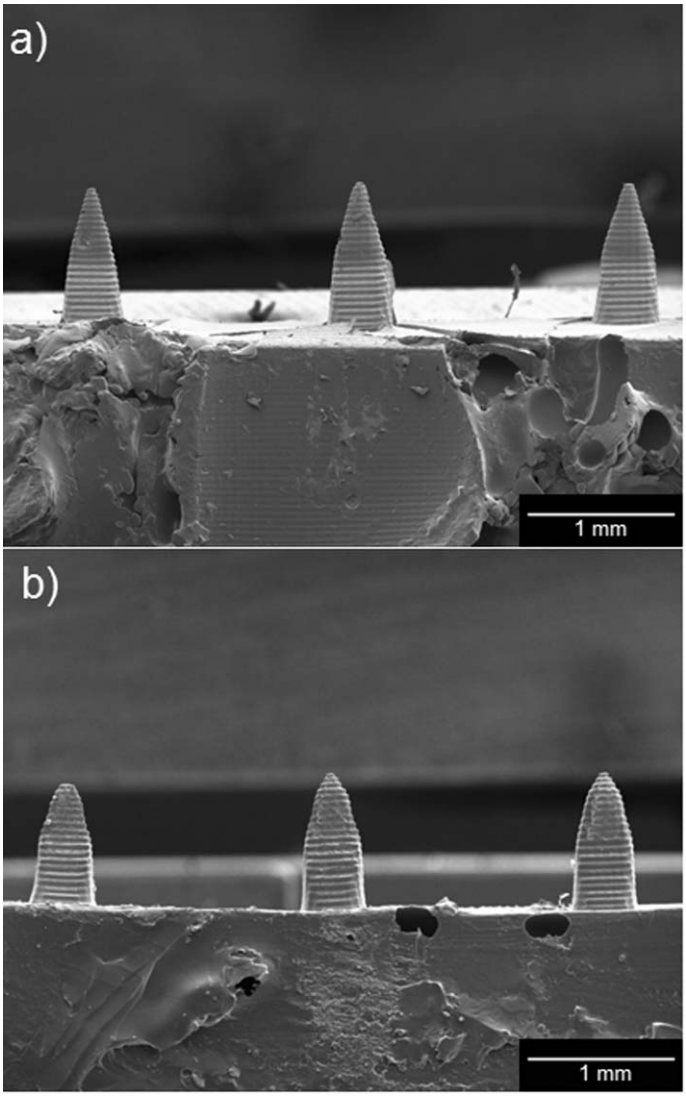

FIG. 3. Scanning electron micrographs of unmodified and quantum dot-coated Gantrez® AN-139 microneedles. (a) Scanning electron micrograph of three unmodified Gantrez® AN-139 polymer microneedles in a five microneedle array; these microneedles were produced using visible light dynamic mask micro-stereolithography-micromolding. (b) Scanning electron micrograph of three quantum dot-coated Gantrez® AN-139 polymer microneedles in a five microneedle array; these microneedles were produced using visible light dynamic mask micro-stereolithography-micromolding and piezoelectric inkjet printing. Triangle-shaped regions, which were modified by the quantum dot solution, can be observed on the longitudinally cut surfaces of the coated microneedles.

More recent work by Zhang *et al.* showed the topically applied quantum dots became localized within the outer layers of the stratum corneum as well as near hair follicles.[76] The reduction in image quality from deeper tissue regions is attributed to deflection by skin tissue, autofluorescence of skin tissue, and poor light penetration.[77] An increase in laser power may facilitate imaging of deeper tissues; however, tissue burning may take place at high laser intensities. Levene *et al.* utilized gradient index lenses with needle-like dimensions to perform multiphoton microscopy of deep tissues; for example, they obtained images of quantum dots within hippocampal and cortical layer tissues in a murine model.[78] Other techniques may find use for in vivo imaging of deeper skin layers. For example, Krstajic *et al.* utilized optical coherence tomography for imaging of deeper skin layers; they noted that imaging of tissues greater than 500 μm from the surface was relatively poor.[79]

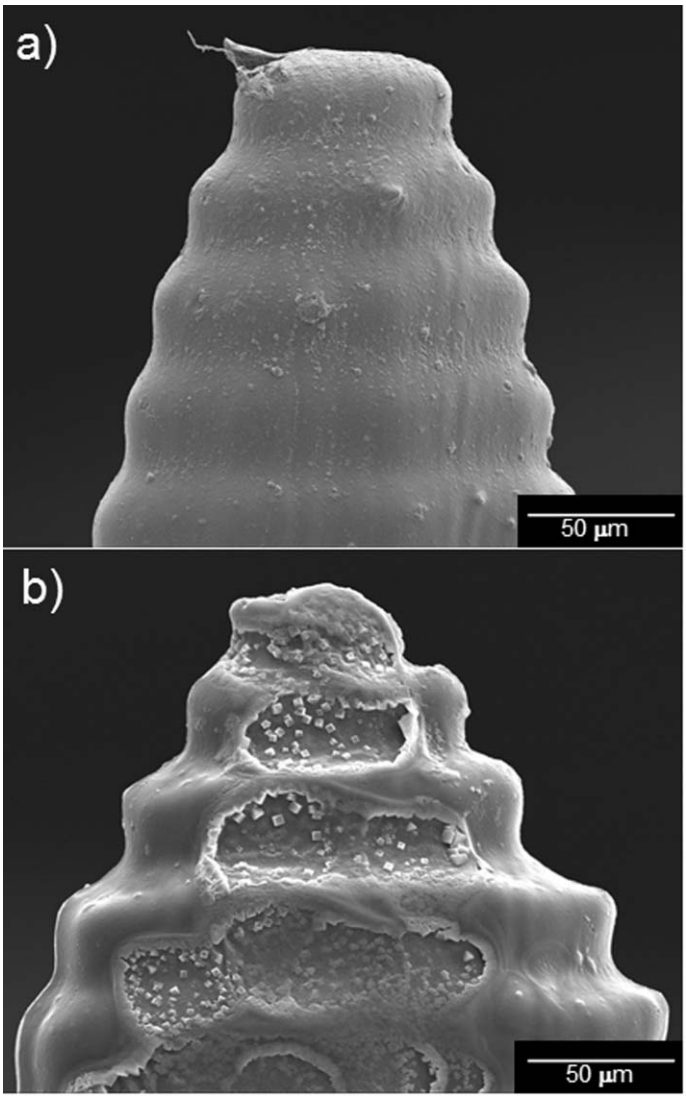

FIG. 4. Scanning electron micrographs of an unmodified Gantrez® AN-139 microneedle and a quantum dot-coated Gantrez® AN-139 microneedle. (a) Scanning electron micrograph of an individual unmodified Gantrez® AN-139 polymer microneedle. (b) Scanning electron micrograph of an individual quantum dot-coated Gantrez® AN-139 polymer microneedle. The longitudinally cut surface of the coated microneedle exhibited crater-like features, which were attributed to hydrolysis of the Gantrez® AN-139 polymer by the quantum dot solution. Sodium chloride crystal precipitation from phosphate buffered saline solution was observed on the coated microneedle surface.

IV. CONCLUSIONS

We successfully modified the surfaces of solid Gantrez® AN-139 polymer microneedles by means of piezoelectric inkjet printing. The Young's modulus value for Gantrez® AN-139 suggests that it has appropriate stiffness for use in microneedle-based transdermal drug delivery. Deposition of quantum dot solution onto Gantrez® AN-139 microneedles was confirmed via scanning electron microscopy. The quantum dot-coated Gantrez® AN-139 microneedle successfully created a pore in the stratum corneum layer, which enabled delivery of quantum dots to deeper layers of the skin. Multiphoton imaging indicated that quantum dots were placed >200 μm within the skin by the quantum dot-coated Gantrez® AN-139 polymer microneedle.

This study provides a proof-of-concept involving the combination of two rapid prototyping methods, visible light dynamic mask micro-stereolithography-micromolding and inkjet printing, for

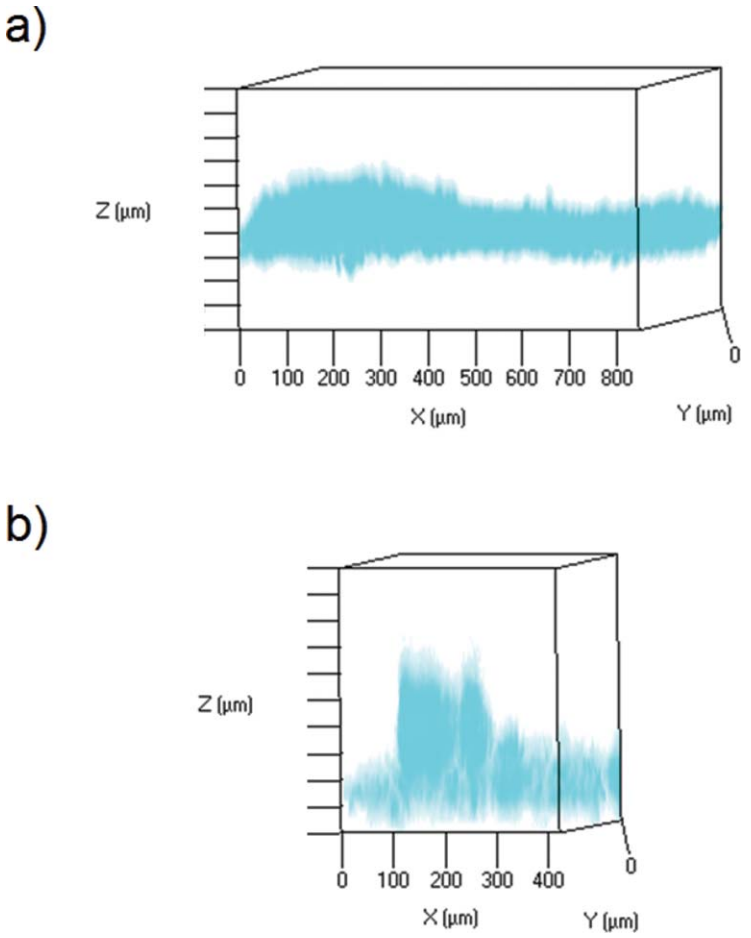

FIG. 5. Maximum projections (in red) rendered from acquired z-stack multiphoton images of quantum dot delivery into porcine skin. (a) Topically applied quantum dots one hour after application. The skin was oriented with the stratum corneum at the top of the imaging window. (b) A single microneedle one hour after application. The image was oriented with the microneedle and the stratum corneum at the bottom of the imaging window. In these figures, the spacing between the bars on the Z-axis is 50 μm. Inversion of the colors was performed to facilitate viewing.

fabrication of biodegradable microneedles. This approach is associated several attributes, including rapid processing times, scalability, and low cost. It should be noted that no high-cost processing environments, such as clean room environments, are necessary for microneedle fabrication using this approach. The combination of visible light dynamic mask micro-stereolithography-micromolding and inkjet printing enables fabrication of solid microneedles containing a wide range of geometries as well as a wide range of pharmacologic agent compositions. For example, inkjet printing may be a useful approach for incorporating highly lipophilic pharmacologic agents (e.g., photosensitizers) on solid microneedles. Printing of multiple agents, including proteins and nucleic acids, on microneedles may enable the development of transdermal sensors and theranostic (combined detection and treatment) devices. In addition, visible light dynamic mask micro-stereolithography-micromolding and inkjet printing may be used to fabricate microneedles for patient-specific applications, including usage in depth-dependent transdermal delivery (e.g., precise delivery of pharmacologic agents to epidermal, dermal, or subdermal tissues). The development of additional coating materials that enable dissolution of pharmacologic agents and exhibit compatibility with inkjet cartridge materials would facilitate this work. The functionality and biodistribution of pharmacologic agents after inkjet printing also needs to be considered. We envision that devices containing inkjet printer-modified microneedles and sensors may be used for treatment of diabetes mellitus and other chronic medical conditions.

ACKNOWLEDGMENTS

We would like to acknowledge B Andersen, C Mooney, and J Schwartz for assistance with Fourier transform infrared spectroscopy, scanning electron microscopy, and multiphoton microscopy, respectively.

[1] S. D. Gittard, A. Ovsianikov, B. N. Chichkov, A. Doraiswamy, R. J. Narayan, Expert Opinion on Drug Delivery **7**, 21 (2010).
[2] M. R. Prausnitz, Advanced Drug Delivery Reviews **56**, 581 (2004).
[3] M. R. Prausnitz, S. Mitragotri, and R. Langer, Nature Reviews Drug Discovery **3**, 115 (2004).
[4] F. Chabri, K. Bouris, T. Jones, D. Barrow, A. Hann, C. Allender, K. Brain, and J. Birchall, British Journal of Dermatology **150**, 869 (2004).
[5] W. Lin, M. Cormier, A. Samiee, A. Griffin, B. Johnson, C. L. Teng, G. E. Hardee, and P. E. Daddona, Pharmaceutical Research **18**, 1789 (2001).
[6] J. Birchall, S. Coulman, M. Pearton, C. Allender, K. Brain, A. Anstey, C. Gateley, N. Wilke, and A. Morrissey, Journal of Drug Targeting **13**, 415 (2005).
[7] H. S. Gill, D. D. Denson, B. A. Burris, and M. R. Prausnitz, Clinical Journal of Pain **24**, 585 (2008).
[8] S. el Khafagy, M. Morishita, Y. Onuki, and K. Takayama, Advanced Drug Delivery Reviews **59**, 1521 (2007).
[9] Y. B. Schuetz, A. Naik, R. H. Guy, and Y. N. Kalia, Expert Opinion on Drug Delivery **2**, 533 (2005).
[10] H. S. Gill and M. R. Prausnitz, Journal of Controlled Release **117**, 227 (2007).
[11] M. Cormier, B. Johnson, M. Ameri, K. Nyam, L. Libiran, D. D. Zhang, and P. Daddona, Journal of Controlled Release **97**, 503 (2004).
[12] J. A. Matriano, M. Cormier, J. Johnson, W. A. Young, M. Buttery, K. Nyam, and P. E. Daddona, Pharmaceutical Research **19**, 63 (2002).
[13] G. Widera, J. Johnson, L. Kim, L. Libiran, K. Nyam, P. E. Daddona, M. Cormier, Vaccine **24**, 1653 (2006).
[14] H. S. Gill and M. R. Prausnitz, Pharmaceutical Research **24**, 1369 (2007).
[15] X. Chen, H. J. Corbett, S. R. Yukiko, A. P. Raphael, E. J. Fairmaid, T. W. Prow, L. E. Brown, G. J. P. Fernando, M. A. F. Kendall, Advanced Functional Materials **21**, 464 (2011).
[16] M. Cerna, M. Vesely, and P. Dzik, Catalysis Today **161**, 97 (2011).
[17] R. D. Boehm, S. D. Gittard, J. M. H. Byrne, A. Doraiswamy, J. J. Wilker, T. M. Dunaway, R. Crombez, W. Shen, Y. S. Lee, and R. J. Narayan, JOM **62**, 56 (2010).
[18] A. Doraiswamy, T. M. Dunaway, J. J. Wilker, and R. J. Narayan, Journal of Biomedical Materials Research Part B-Applied Biomaterials **89B**, 28 (2009).
[19] J. D. Kim, J. S. Choi, B. S. Kim, Y. C. Choi, and Y. W. Cho, Polymer **51**, 2147 (2010).
[20] P. C. Chang, J. Lee, D. Huand, V. Subramanian. A. R. Murphy, and J. M. J. Frechet, Chemistry of Materials **16**, 4783 (2004).
[21] K. Abe, J. Suzuki, and D. Citterio, Analytical Chemistry **80**, 6928 (2008).
[22] L. R. Allain, D. N. Stratis-Cullum, and T. Vo-Dinh, Analytica Chimica Acta **518**, 77 (2004).
[23] P. Dzik, M. Vesely, and J. Chomoucka, Journal of Advanced Oxidation Technologies **13**, 172 (2010).
[24] S. T. Lin, M. H. Chang, J. B. Horng, H. L. Cheng, and W. Y. Chou, in *Organic Light Emitting Materials and Devices XI* (Proceedings Vol. **6655**), 2007 (doi: 10.1117/12.733253).
[25] M. Mosiadz, R. I. Tomov, S. C. Hopkins, G. Martin, D. Hardeman, B. Holzapfel, and B. A. Glowacki, Journal of Sol-Gel Science and Technology **54**, 154 (2010).
[26] R. Saunders and B. Derby, in *Encyclopedia of Industrial Biotechnology: Bioprocess, Bioseparation, and Cell Technology*, edited by M. C. Flickinger (John Wiley & Sons, Hoboken, 2010).
[27] J. Sumerel, J. Lewis, A. Doraiswamy, L. F. Deravi, S. L. Sewell, A. E. Gerdon, D. W. Wright DW, R. J. Narayan, Biotechnol Journal **1**, 976 (2006).
[28] J. H. Park, M. G. Allen, and M. R. Prausnitz, Journal of Controlled Release **104**, 51 (2005).
[29] P. M. Wang, M. Cornwell, J. Hill, and M. R. Prausnitz, Journal of Investigative Dermatology **126**, 1080 (2006).
[30] H. S. Gill and M. R. Prausnitz, Journal of Controlled Release **117**, 227 (2007).
[31] S. D. Gittard, P. R. Miller, B. D. Boehm, A. Ovsianikov, B. N. Chichkov, J. Heiser, J. Gordon, N. A. Monteiro-Riviere, and R. J. Narayan, Faraday Discussions **149**, 171 (2011).
[32] L. C. Lappas and W. McKeehan, Journal of Pharmaceutical Sciences **54**, 176 (1965).
[33] M. Glicksman in *Advanced in Food Research*, edited by G. F. Stewart (Academic Press, New York, 1963).
[34] J. M. Irache, M. Huici, M. Konecy, S. Espuela, M. A. Campanero, and P. Arbos, Molecules **10**, 126 (2005).
[35] I. Corzani, U. S. Patent No. 6403113 (11 June, 2002).
[36] S. D. Gittard, R. J. Narayan, C. Jin, A. Ovsianikov, B. N. Chichkov, N. A. Monteiro-Riviere, S. Stafslien, and B. Chisholm, Biofabrication **1**, 041001 (2009).
[37] S. D. Gittard, A. Ovsianikov, H. Akar, B. Chichkov, N. A. Monteiro-Riviere, S. Stafslien, B. Chisholm, C. C. Shin, C. M. Shih, S. J. Lin, Y. Y. Su, and R. J. Narayan, Advanced Engineering Materials **12**, B77 (2010).
[38] P. V. Date, A. Samad, and P. V. Devarajan, AAPS PharmSciTech **11**, 304 (2010).
[39] E. Elizondo, S. Sala, E. Imbuluzqueta, D. Gonzalez, M. J. Blanco-Prieto, C. Gamazo, N. Ventosa, and J. Venciana, Pharmaceutical Research **28**, 309 (2011).
[40] N. Nabi, C. Mukerjee, R. Schmid, A. Gaffar, American Journal of Dentistry **2**, 197 (1989).
[41] F. S. Panagakos, A. R. Volpe, M. E. Petrone, W. DeVizio, and R. M. Davies, Journal of Clinical Dentistry **16**, S1 (2005).
[42] R. F. Donnelly, R. Majithiya, T. R. R. Singh, D. I. J. Morrow, M. J. Garland, Y. K. Demir, K. Migalska, E. Ryan, D. Gillen, C. J. Scott, and A. D. Woolfson, Pharmaceutical Research **28**, 41 (2011).

[43] R. F. Donnelly, D. I. J. Morrow, F. Fay, C. J. Scott, S. Abdelghany, R. R. T. Singh, M. J. Garland, and A. D. Woolfson, Photodiagnosis and Photodynamic Therapy **7**, 222 (2010).
[44] M. Bruchez, M. Moronne, P. Gin, S. Weiss, and A. P. Alivisatos, Science 281 (1998).
[45] C. M. Niemeyer, Angewandte Chemie International Edition **40**, 4128 (2001).
[46] E. Klarreich, Nature **413**, 450 (2001).
[47] C. Seydel, Science **300**, 80 (2003).
[48] Y. Ho and K. W. Leong, Nanoscale **2**, 60 (2010).
[49] H. Tada, H. Higuchi, T. M. Wanatabe, and N. Ohuchi, Cancer Research **67**, 1138 (2007).
[50] A. M. Derfus, A. A. Chen, D. Min, E. Ruoslahti, and S. N. Bhatia, Bioconjugate Chemistry **18**, 1391 (2007).
[51] S. Dwarakanath, J. G. Bruno, A. Shastry, T. Phillips, A. John, A. Kumar, and L. D. Stephenson, Biochemical and Biophysical Research Communications **325**, 739 (2004).
[52] Y. Li, Z. He, P. Zhang, J. Gao, C. Cheng, and H. Zhang, Journal of Nanoscience and Nanotechnology **10**, 520 (2010).
[53] V. Bagalkot, L. Zhang, E. Levy-Nissenbaum, S. Jon, P. W. Kantoff, R. Langer, and O. C. Farokhzad, Nano Letters **7**, 3065 (2007).
[54] W. Cai and X. Chen, Nature Protocols **3**, 89 (2008).
[55] I. Park, Y. M. Ha, and S. H. Lee, International Journal of Advanced Manufacturing Technology **46**, 151 (2010).
[56] P. R. Miller, S. D. Gittard, T. L. Edwards, D. M. Lopez, X. Xiao, D. R. Wheeler, N. A. Monteiro-Riviere, S. M. Brozik, R. Polsky, and R. J. Narayan, Biomicrofluidics **5**, 013415 (2011).
[57] Technical Data: EnvisionTEC e-Shell 200 Series. http://www.envisiontec.de/fileadmin/pdf/matsheet_eshell200_en_s.pdf. Retrieved 11 April 2011.
[58] Gantrez® AN-139. http://online1.ispcorp.com/en-US/Pages/ProductDetail.aspx?BU=Performance%20Chemicals&l1=Textiles&prodName=Gantrez%C2%AE%20AN-139&prdId=74014. Retrieved 11 April 2011.
[59] R. C. Rowe, P. J. Sheskey, and S. C. Owen, *Handbook of Pharmaceutical Excipients*, Part 3. (Pharmaceutical Press, Gurnee, IL, 2006).
[60] C. H. Lin, L. W. Chang, H. Chang, M. H. Yang, C. S. Yang, W. H. Lai, W. H. Chang, and P. Lin, Nanotechnology **20**, 215101 (2009).
[61] Qtracker® non-targeted quantum dots for in vivo imaging http://probes.invitrogen.com/media/pis/mp19011.pdf. Retrieved 11 April 2011.
[62] L. W. Zhang and N. A. Monteiro-Riviere, Skin Pharmacology and Physiology **21**, 166 (2008).
[63] N. A. Monteiro-Riviere, A. O. Inman, and J. P. Ryman-Rasmussen, in *Nanotoxicology: Characterization, Dosing, and Health Effects*, edited by N. A. Monteiro-Riviere and C. L. Tran (Informa Healthcare, New York, 2007).
[64] J. P. Ryman-Rasmussen, J. E. Riviere, and N. A. Monteiro-Riviere, Toxicological Sciences **81**, 159 (2006).
[65] W. C. Oliver and G. M. Pharr, Journal of Materials Research **7**, 1564 (1992).
[66] W. Meyer, R. Schwarz, and K. Neurand, Current Problems in Dermatology **7**, 39 (1978).
[67] N. A. Monteiro-Riviere and J. E. Riviere, in *Advances In Swine In Biomedical Research*, edited by M. E. Tumbleson and L. B. Schook (Plenum Publishing Corporation, New York, 1996), Vol.**II**, pp. 425-458.
[68] N. A. Monteiro-Riviere, in *Swine in Biomedical Research*, edited by M. E. Tumbleson (Plenum Publishing Corporation, New York, 1986), Vol. **I**, pp. 641-655.
[69] N. A. Monteiro-Riviere, in *The Biology of the Domestic Pig*, edited by W. G. Pond and H. J. Mersmann (Cornell University Press, Ithaca, NY, 2001).
[70] R. Weissleder and M. J. Pittet, Nature **452**, 580 (2008).
[71] D. R. Larson, W. R. Zipfel, R. M. Williams, S. W. Clark, M. P. Bruchez, F. W. Wise, and W. W. Webb, Science **300**, 1434 (2003).
[72] Y. Kim, P. J. Ludovice, and M. R. Prausnitz, Journal of Controlled Release **122**, 375 (2007).
[73] J. H. Park, M. G. Allen, and M. R. Prausnitz, Journal of Controlled Release **104**, 51 (2005).
[74] J. H. Park and M. R. Prausnitz, Journal of the Korean Physical Society **56**, 1223 (2010).
[75] The Infrared Spectroscopy Committee of the Chicago Society for Coatings Technology, *An infrared spectroscopy atlas for the coatings industry* (Federation of Societies for Coatings Technology, Philadelphia, PA, 1980), pp. 269.
[76] L. W. Zhang, W. W. Yu, V. L. Colvin, and N. A. Monteiro-Riviere, Toxicology and Applied Pharmacology **228**, 200 (2008).
[77] General discussion, Faraday Discussions **149**, 227 (2011).
[78] M. J. Levene, D. A. Dombeck, K. A. Kasischke, R. P. Molloy, and W. W. Webb, Journal of Neurophysiology **91**, 1908 (2004).
[79] N. Krstajic, L. E. Smith, S. J. Matcher, D. T. D. Childs, M. Bonesi, P. D. L. Greenwood, M. Hugues, K. Kennedy, M. Hopkinson, K. M. Groom, S. MacNeil, R. A. Hogg, and R. Smallwood, IEEE Journal of Selected Topics in Quantum Electronics **16**, 748 (2010).